Am J Cancer Res 2021;11(10):4768-4787
www.ajcr.us /ISSN:2156-6976/ajcr0137702

Original Article

Breast Cancer Antiestrogen Resistance 3 (BCAR3) promotes tumor growth and progression in triple-negative breast cancer

Janet Arras[1*], Keena S Thomas[1*], Paul J Myers[2], Allison M Cross[1], Amare D Osei[1], Gabriel E Vazquez[1], Kristen A Atkins[3], Mark R Conaway[4], Marieke K Jones[5], Matthew J Lazzara[2], Amy H Bouton[1]

[1]Department of Microbiology, Immunology and Cancer Biology, University of Virginia School of Medicine and Cancer Center, Charlottesville, VA 22908, USA; [2]Department of Chemical Engineering, University of Virginia, Charlottesville, VA 22904, USA; [3]Department of Pathology, University of Virginia School of Medicine and Cancer Center, Charlottesville, VA 22908, USA; [4]Department of Public Health Sciences, University of Virginia School of Medicine and Cancer Center, Charlottesville, VA 22908, USA; [5]Claude Moore Health Sciences Library, University of Virginia, Charlottesville, VA 22908, USA. [*]Equal contributors.

Received July 26, 2021; Accepted September 9, 2021; Epub October 15, 2021; Published October 30, 2021

Abstract: Triple-Negative Breast Cancers (TNBCs) constitute roughly 10-20% of breast cancers and are associated with poor clinical outcomes. Previous work from our laboratory and others has determined that the cytoplasmic adaptor protein Breast Cancer Antiestrogen Resistance 3 (BCAR3) is an important promoter of cell motility and invasion of breast cancer cells. In this study, we use both *in vivo* and *in vitro* approaches to extend our understanding of BCAR3 function in TNBC. We show that BCAR3 is upregulated in ductal carcinoma *in situ* (DCIS) and invasive carcinomas compared to normal mammary tissue, and that survival of TNBC patients whose tumors contained elevated BCAR3 mRNA is reduced relative to individuals whose tumors had less BCAR3 mRNA. Using mouse orthotopic tumor models, we further show that BCAR3 is required for efficient TNBC tumor growth. Analysis of publicly available RNA expression databases revealed that MET receptor signaling is strongly correlated with BCAR3 mRNA expression. A functional role for BCAR3-MET coupling is supported by data showing that both proteins participate in a single pathway to control proliferation and migration of TNBC cells. Interestingly, the mechanism through which this functional interaction operates appears to differ in different genetic backgrounds of TNBC, stemming in one case from potential differences in the strength of downstream signaling by the MET receptor and in another from BCAR3-dependent activation of an autocrine loop involving the production of HGF mRNA. Together, these data open the possibility for new approaches to personalized therapy for individuals with TNBCs.

Keywords: BCAR3, tyrosine kinase signaling, adhesion signaling, MET receptor, Foretinib

Introduction

With the advent of the genomic era, it has become increasingly clear that breast cancers comprise a collection of diseases influenced by distinct molecular and genetic drivers as well as systemic and microenvironmental factors. Cell-intrinsic signaling networks play a critical role in integrating external cues with genetic programs that contribute to tumor growth and progression. Previous work from our group has shown that the adaptor molecule Breast Cancer Antiestrogen Resistance 3 (BCAR3) functions within these signaling networks to control cell adhesion, migration, and invasion of breast cancer cells [1, 2]. BCAR3 was originally identified in a screen for genes implicated in resistance to antiestrogens in estrogen receptor-positive (ER+) breast cancer cell lines [3]. At its N-terminus, BCAR3 contains a Src-homology 2 (SH2) domain that has been reported to bind to Protein Tyrosine Phosphatase α (PTPα) and human epidermal growth factor receptor 3 (HER3). Its C-terminus contains a domain that mediates binding to the adaptor molecule $p130^{Cas}$ (Cas) and has homology to the guanine nucleotide exchange factor (GEF) domain of Cdc25 [3-7]. This domain adopts a closed cata-

Table 1. Cell lines used in this study

Cell line	Source	Media[1]	Supplements[1]
Hs578T	ATCC[5]	High-glucose DMEM[2]	0.01 mg/mL bovine insulin[3]; 10% FBS[4]; 1% penicillin-streptomycin
MDA-MB-231	ATCC	High-glucose DMEM	10% FBS; 1% penicillin-streptomycin
BT-549	ATCC	High-glucose DMEM	10% FBS; 1% penicillin-streptomycin
MDA-MB-157	ATCC	Leibovitz's L-15 (CO_2-free)	10% FBS; 1% penicillin-streptomycin
MDA-MB-468	ATCC	Leibovitz's L-15 (CO_2-free)	10% FBS; 1% penicillin-streptomycin
MDA-MB-436	ATCC	Leibovitz's L-15 (CO_2-free)	0.01 mg/mL bovine insulin; 16 µg/mL glutathione; 10% FBS; 1% penicillin-streptomycin
HCC1937	ATCC	RPMI[2]	10% FBS; 1% penicillin-streptomycin
HCC1143	ATCC	RPMI	10% FBS; 1% penicillin-streptomycin
HCC1187	ATCC	RPMI	10% FBS; 1% penicillin-streptomycin
HCC1395	ATCC	RPMI	10% FBS; 1% penicillin-streptomycin
BT-20	ATCC	Eagle's MEM	10% FBS; 1% penicillin-streptomycin

[1]All media and supplements were purchased from Gibco Life Technologies, Carlsbad, CA, USA unless otherwise noted. [2]DMEM: Dulbecco's Modified Eagle's Medium; RPMI: Roswell Park Memorial Institute. [3]Bovine insulin from Sigma-Aldrich, St. Louis, MO, USA. [4]FBS: fetal bovine serum. [5]ATCC: American Type Culture Collection, Manassas, VA, USA.

lytically inactive conformation that impedes GEF activity while facilitating binding to Cas [5]. BCAR3-Cas interactions enhance the activity of the non-receptor tyrosine kinase c-Src (Src) and positively regulate cell adhesion, invasion, proliferation, and activation of the small GTPase Rac1 [1, 8-12].

Similar to BCAR3, Cas, and Src, the MET receptor tyrosine kinase modulates cell migration, invasion, and growth through its interactions with hepatocyte growth factor/scatter factor (HGF/SF) [13-15]. MET and HGF/SF have also been reported to create an autocrine signaling loop that is important for the tumorigenic functions associated with MET in cancers [16]. MET receptor protein expression is elevated in 15-20% of breast cancer cases and is associated with poor outcomes across several breast cancer subtypes, including triple-negative breast cancer (TNBC) [17-20]. Elevated levels of active (autophosphorylated) and total MET protein correlate with a poor prognosis in patients with breast cancer [21]. In addition, over-expression of MET and HGF/SF has been reported in patient-derived invasive breast cancer tissues [22], and elevated levels of circulating HGF/SF in patient serum is associated with recurrence and reduced survival in patients with breast cancer [23].

In the current study, we extend our understanding of BCAR3 function in TNBC. We show that BCAR3 is upregulated in ductal carcinoma *in situ* (DCIS) and invasive TNBC compared to normal mammary tissue, and that BCAR3 mRNA expression is associated with poor survival for patients with TNBC. In mice, BCAR3 is required for TNBC tumor growth. Finally, using multiple cell models, we show that BCAR3 promotes TNBC cell proliferation, autocrine growth control, and migration through signaling pathways that include the MET receptor. These data underscore the potential utility of BCAR3 as a gateway into new targetable pathways for the treatment of TNBC.

Materials and methods

Histological staining and microarray analysis

Formalin-fixed, paraffin-embedded (FFPE) mammary tumor samples were obtained from the Biorepository and Tissue Research Facility at UVA. Serial sections were stained with hematoxylin and eosin (H&E) or immunostained with BCAR3 antibodies. Specificity was established by parallel staining of control and BCAR3-depleted MDA-MB-231 FFPE cell pellets. Microarrays containing core biopsies were described in Dill *et al.* [24].

Patient survival analysis

The Kaplan-Meier Plotter algorithm [25] was used to compare survival of patients whose tumors fell in the top quartile of BCAR3 expression to the remaining patients in the full dataset of 255 TNBC patients.

Cell culture

Breast cancer cell lines used in this study are shown in **Table 1**.

Ectopic expression and knockdown of BCAR3

Stable MDA-MB-231 and Hs578T BCAR3 knockdown and re-expression cell lines were

Table 2. Antibodies used in this study

Protein	Species	Catalogue #	Company	Location
ERK 1/2	Rabbit	9102	Cell Signaling Technology	Danvers, MA, USA
BCAR3	Rabbit	HPA 014858	Sigma-Aldrich	St. Louis, MO, USA
MET	Mouse	3127	Cell Signaling Technology	Danvers, MA, USA
pMET (pTyr1234/1235)	Mouse	3077	Cell Signaling Technology	Danvers, MA, USA
GAPDH	Mouse	Sc-32233	Santa Cruz	Dallas, TX, USA

generated via lentiviral transduction using small hairpin RNAs targeting BCAR3 [1]. shBCAR3-1 and shBCAR3-2 oligonucleotides targeting BCAR3 were generated and cloned into the TRC2-pLKO-puro vector (Sigma-Aldrich, St. Louis, Mo, USA). The following hairpin sequences were used: shBCAR3-1 shRNA ID: TRCN0000364816, sequence: 5'-CCGGTAAC TGCCCTCTCGCGTAAATCTCGAGATTTACGCGA GAGGGCAGTTATTTTTG-3'. shBCAR3-2 shRNA ID: TRC0000376503, sequence: 5'-CCGGTC GGCATTGCAGTGGACATTCCTCGAGGAATGTCCA CTGCAATGCCGATTTTTG-3'.

shBCAR3-1 knockdown cell lines were used to generate control and BCAR3 re-expression cells by viral transduction with empty vector (pLV-Venus; shBCAR3 + Ctl) or vector encoding a wobble mutant of wildtype (WT) Venus-BCAR3 (shBCAR3 + WT BCAR3) [1]. Wildtype (WT) BCAR3 complementary DNA was cloned into the *NotI* and *SpeI sites* of the pLV-Venus vector. The QuikChange II XL Site-Directed Mutagenesis Kit (Agilent Technologies, Santa Clara, CA, USA; 200521) was used to perform site directed mutagenesis. The primer sequences used are as follows: shB3wobble1 forward: 5'-CCAGATTTTAACTGCGCTGTCCGAA AATTGGAACCTCCTCCTG-3', shB3wobble1 reverse: 5'-CAGGAGGAGGTTCCAATTTTCGGGAC AGCGCAGTTAAAATCTGG-3' (Changed nucleotides are underlined, and all constructs were confirmed by sequencing). shBCAR3 + Ctl and shBCAR3 + WT BCAR3 cells were then sorted by flow cytometry to obtain the population of cells with the highest expression of Venus. All engineered cell lines were cultured as stated above and maintained in 0.5 μg/ml (MDA-MB-231 cells) and 1 μg/ml (Hs578T cells) puromycin (MP Biomedicals, Santa Ana, CA, USA; 100552). Doxycycline (Dox)-inducible shBCAR3 knockdown constructs were generated using the Tet-on 3G bidirectional inducible expression system (Takara, San Jose, CA, USA). BCAR3 knockdown was induced in these cells by the addition of 1 μg/ml Dox (MP Biomedicals, Irvine, CA, USA; ICN19895505) in the medium (*in vitro*) or 1 mg/mL Dox plus 0.4% sucrose in the drinking water of mice (*in vivo*).

Tumor xenografts

Six-week old homozygous Foxn1$^{nu/nu}$ female mice (Jackson Laboratories, Bar Harbor, ME, USA) were anesthetized by intraperitoneal (IP) injection of 6 mg/25 g body weight tribromoethanol and injected bilaterally with 2×10^6 tumor cells into each 4th inguinal mammary fat pad. To induce conditional knockdown of BCAR3 in the Dox-inducible conditional knockdown cells, drinking water was supplemented with 1 mg/mL Dox plus 0.4% sucrose when tumors reached 200 mm^3. Tumor growth was monitored weekly by caliper until tumors became palpable, and then 3 times a week thereafter. Mice were euthanized once humane endpoints were reached. Tumors were then excised and processed for immunohistochemistry. All animal work was performed in accordance with established guidelines, and following approval by, the University of Virginia Animal Care and Use Committee.

Immunoblotting

Immunoblots were performed as described previously [1, 2]. Antibodies are shown on **Table 2**.

Organoid cultures

Primary mammary organoids were generated using epithelial cells obtained from mouse mammary glands isolated from WT and BCAR3 KO (gift from Dr. Adam Lerner) [26] 8-week-old mice as described by Nguyen-Ngoc, *et al.* [27]. Epithelial cell suspensions were plated on growth factor-reduced Matrigel (Corning, Corning, NY, USA; 354230) and cultured in DMEM/F12 media supplemented with 2.5 nM FGF2 (PeproTech, Rocky Hill, NJ, USA; 100-18B) or 9

nM TGFα (Sigma-Aldrich; T7924) for 7 days with a media change every 3-4 days.

Cell proliferation and colony growth

Cells were plated in 8 separate 96-well plates at a density of 1,000 cells per well for analysis using the CyQUANT NF Cell Proliferation Assay Kit (Invitrogen, Waltham, MA, USA; C35007). Samples were processed at 6 hours post-plating and every day thereafter for 7 days with no media changes. Fold-change was determined by calculating the average fluorescence (excitation at ~485 nm and emission detection at ~530 nm) of 4-6 technical replicates per cell line at each day relative to 6 hours.

To measure colony growth, 1,000 cells were plated in triplicate wells of a 6-well plate and grown for 10 (MDA-MB-231 cells) or 15 (Hs578T cells) days with no media changes. Cells were fixed with 3% paraformaldehyde, stained with a 0.05% crystal violet solution in methanol overnight, washed with 1X PBS, and left to dry. Plates were scanned using the ChemiDoc imaging system (Bio-Rad, Hercules, CA, USA) and signal intensity per unit area was quantified by ImageJ (NIH, Bethesda, MD, USA; version 1.51).

To measure the effect of HGF on colony growth, cells were plated, allowed to adhere for 24 hours and treated with either 0.05% BSA (vehicle) or 50 ng/mL HGF and supplemented every 3 days (MDA-MB-231) or one time 3 days after plating (Hs578T). Images were processed in ImageJ by applying a median filter of 2 pixels and a color threshold. The area of all detected colonies was measured in mm^2 using the ImageJ particle analysis tool. Colony areas for each condition were compiled and the distribution of colony size for each condition was analyzed. Using quartile data obtained from the distribution present in vehicle-treated Vector-control cells, colony sizes for each condition were separated into large, average, and small for statistical analysis.

To assess MET activation, cells were plated at a density of 2.5×10^5, 1.25×10^5, and 2.5×10^4 cells per 60 mm dish and cultured for 2, 5, and 10 days, respectively, with no media changes.

Survival assay

Cells were plated at a density of 1.5×10^5 or 2.5×10^5 cells per 6-well plate in the presence of DMSO (vehicle) or 50 nM Foretinib, and cultured for 72 hours and 24 hours, respectively. Cells were trypsinized and cell viability measured using Trypan Blue exclusion (Thermo Scientific; Waltham, MA, USA; SV30084.01).

Gene set variation analysis (GSVA)

RNA expression data from the Cancer Cell Line Encyclopedia (CCLE) for 32 TNBC cell lines were downloaded from the Cancer Dependency Map (DepMap, release 21Q2; https://depmap.org/portal/download/). GSVA [28] was then used to calculate enrichment scores for the Reactome gene sets [29] related to receptor tyrosine kinase signaling. Spearman rank correlation coefficients were calculated for each set of GSVA scores against BCAR3 transcript expression from the 32 TNBC cell lines. Rank correlations and *P*-values were calculated using the Hmisc R package. R version 4.1.0 was used in these analyses. The codes for these analyses are available on GitHub under the username “pauljmyers”.

Transwell migration assay

Transwell migration assays were performed as previously described [2]. Cells were suspended in FBS-free DMEM and seeded at 2.5×10^4 cells per well in the upper chamber of the Transwell chamber (Costar 3422, 8 μm pore size) in the presence of DMSO (vehicle) or 50 nM Foretinib. The lower chamber was filled with DMEM supplemented with 10% FBS and 50 ng/mL HGF (PeproTech, 100-39H). Boyden chambers were incubated for 6 hours after which cells on the bottom surface were stained using Protocol HEMA 3 stain set (Fisher Scientific, Waltham, MA, USA; 122-911) and quantified under the microscope. Data were normalized relative to DMSO-treated Vector-control.

Drug inhibitor assays

Cells were plated at half volume in 12-well plates at a density of 500 cells per well, allowed to adhere for 24 hours, and supplemented with media containing either DMSO (vehicle) or Foretinib (ChemCruz, Dallas, TX, USA; sc364492) to a final concentration of 50 nM. Cells were cultured in the presence or absence of Foretinib for 10 days (MDA-MB-231 cells) or 15 days (Hs578T cells) and processed as described above.

Table 3. Primer sequences for qRT-PCR

Gene	Forward (F) Reverse (R)	Primer Sequences (5'-3')
BCAR3	F	CCACATCTTCTGGACCCAAC
BCAR3	R	CTCCTCCTCCAGCTCCTTCT
HGF	F	CGAGGCCATGGTGCTATACT
HGF	R	ATTGACAGTGCCCCTGTAGC
MET	F	CAGTCGGAGGTTCACTGCAT
MET	R	AATCTGGCTTGCTTTGTGCG
GAPDH	F	AACGTGTCAGTGGTGGACCT
GAPDH	R	TCGCTGTTGAAGTCAGAGGA

Quantitative real-time PCR

Quantitative real-time PCR was performed with the Applied Biosystems StepOnePlusReal-Time PCR System (StepOne Software v2.2.2) (Waltham, MA, USA) and the Power SYBR Green PCR Master Mix (Applied Biosystems, Waltham, MA, USA; 4367659). Cells were plated at a density of 2.5×10^5 cells per 60 mm dish and cultured for 48 hours. mRNA was extracted according to the manufacturer's protocol using the Zymo Research Quick RNA microprep kit (Zymo Research, Irvine, CA, USA; R1050). For each sample, 1 µg of mRNA was reverse-transcribed into cDNA in a 20 µl reaction according to the manufacturer's protocol using the iScript cDNA Synthesis Kit (Bio-Rad, 1708890). The final cDNA product was diluted 5X and subjected to quantitative real-time PCR performed with the Applied Biosystems StepOnePlusReal-Time PCR System (StepOne Software v2.2.2) (Waltham, MA, USA) and the Power SYBR Green PCR Master Mix (Applied Biosystems, Waltham, MA, USA; 4367659) using the following thermal cycling conditions: one initial cycle at 95°C for 10 min; 40 cycles of 15 sec at 95°C and 1 min at 60°C; followed by a melt-curve stage of 95°C for 15 sec, 60°C for 1 min, and 95°C for 15 sec. Relative mRNA expression was calculated using the 2(-ΔΔCt) method where transcript expression was normalized to GAPDH mRNA levels. The sequences of the primers used to amplify the genes are shown in **Table 3**.

Statistical analysis

For the non-inducible mouse tumor xenograft experiment (**Figure 2A**), the average volume of the left and right tumors was used as a unit of analysis. Comparisons between groups for the average tumor volume were made with the two-part models discussed in Albert and Shih [30]. Quadratic mixed models were used for tumor volume after the first detectable tumor. The *P*-values were computed from permutation tests based on 2,000 permutations. For the Dox-inducible mouse tumor xenograft experiments (**Figure 2B**), quadratic mixed models were fit to the post-treatment average tumor volumes. The models included random effects for the intercept, linear, and quadratic terms. F-tests based on contrasts were used to compare groups. The analyses treated the left and right tumors as independent.

For all other experiments, normal distribution of residuals was tested before performing one-way ANOVA followed by either Tukey or Sidak post hoc tests to determine *P*-values. Chi-squared tests were used in experiments that tested distributions. In experiments where proportions were compared, the test of 2-proportions was used followed by the Holm method to correct for multiple testing.

Results

BCAR3 is upregulated in breast cancer tumor samples and TNBC cell lines

While BCAR3 protein has been readily detected in breast cancer cell lines, its expression in clinical breast tumor samples has not been rigorously evaluated. Patient-derived tumor sections and microarrays obtained from the UVA Biorepository were evaluated by immunohistochemistry (IHC) for BCAR3 protein expression. The intensity of BCAR3 staining was scored by 2-3 individuals using a scale from 0 (no staining) to 3+ (high staining) (**Figure 1A** and **1B**). Average BCAR3 expression was elevated in DCIS as well as invasive ductal carcinoma (IDC) (**Figure 1A**), and in both ER+/progesterone receptor (PR)+ and TNBC tumors relative to normal mammary tissue (**Figure 1B**). Focusing specifically on TNBCs, BCAR3 was readily detected by Western blot analysis in both claudin-low and basal-like TNBC cells [31-33] (**Figure 1C**). Kaplan-Meier survival curves generated using the top quartile of BCAR3 mRNA expression in 255 TNBC patients show that elevated BCAR3 expression correlates with worse patient outcomes (**Figure 1D**). These results provide the rationale for exploring a potential role for BCAR3 in TNBC tumor growth and progression.

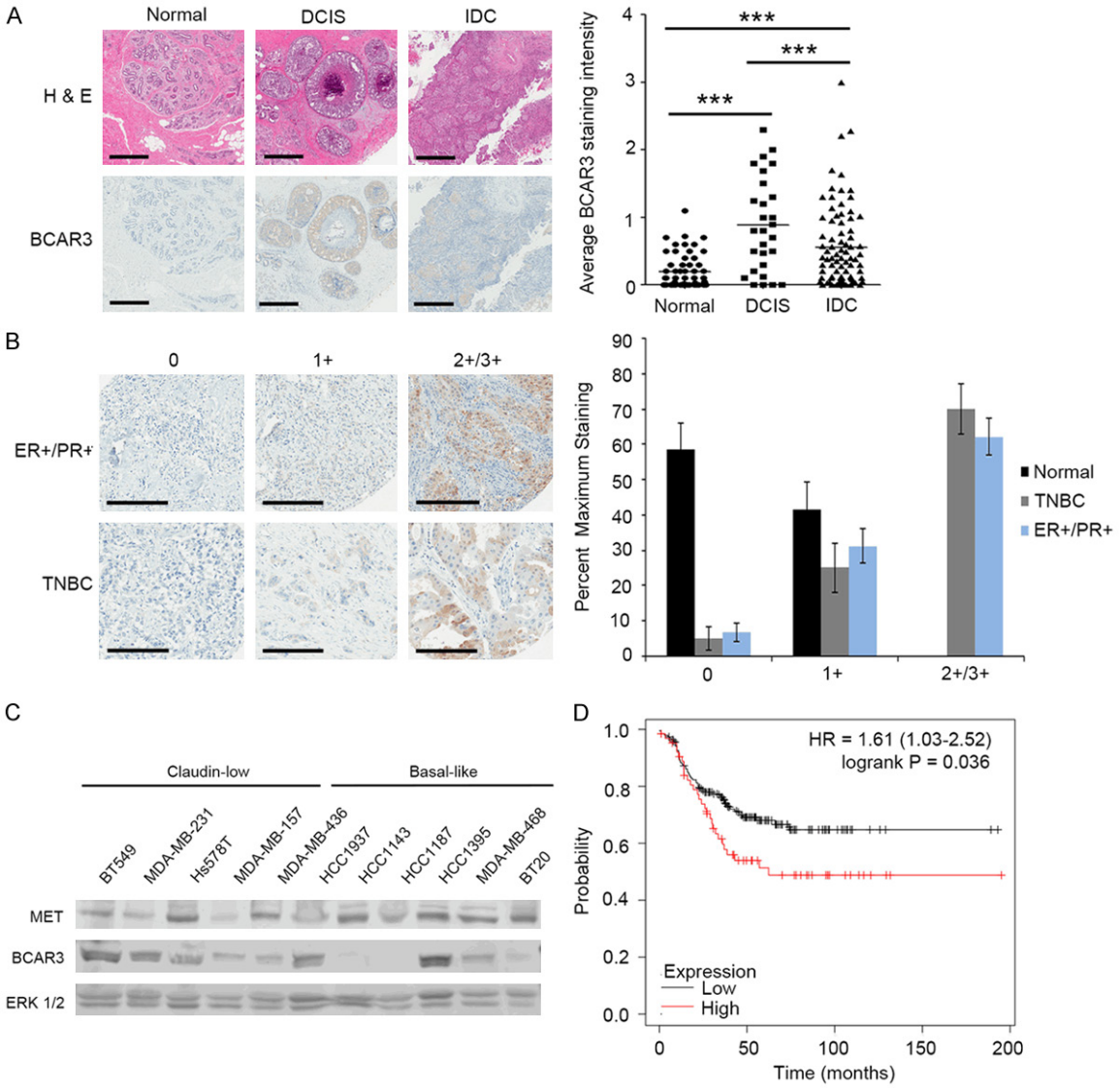

Figure 1. BCAR3 is upregulated in breast cancer samples and TNBC tumor cell lines. (A) Human tissue samples were obtained from the University of Virginia Biorepository and Tissue Research Facility (BTRF) and stained for H&E and BCAR3. Scale bars represent 200 μm. Staining intensity was evaluated by 2-3 investigators on a scale of 0 (no staining) to 3+ (high intensity) (see Panel B below). Data shown are the average of 10 fields per sample for 56 normal breast tissues samples, 28 DCIS samples, and 82 IDC samples. The Kruskal-Wallis test was used to determine differences between groups. ***indicates P<0.0001. (B) Examples of BCAR3 staining intensities from breast tissue microarray samples obtained from the BTRF. Scale bars represent 200 μm. The maximum intensity for BCAR3 staining was assessed by 2-3 investigators in 41 normal samples, 40 TNBC samples and 91 ER+/PR+ samples. Data shown are the percentage of samples exhibiting the indicated maximum staining intensities +/- SEM. (C) Representative immunoblot from 11 TNBC cell lines. Lysates from 40,000 cells were separated by SDS-PAGE and immunoblotted for BCAR3, MET, and ERK 1/2. Samples were derived from the same experiment and processed in parallel on multiple blots. (D) Kaplan-Meier plot showing survival data for 255 TNBC patients separated by the top (red) or remaining (black) quartiles of BCAR3 expression in the primary tumor (https://kmplot.com/analysis/index.php?p=service&start=1) [25].

BCAR3 promotes TNBC tumor growth in vivo

The correlation between BCAR3 expression and poor outcomes in patients with TNBC led us to hypothesize that BCAR3 might influence TNBC tumor growth *in vivo*. This was tested using orthotopic tumor models in which MDA-MB-231 TNBC cells that express endogenous BCAR3 (Vector), reduced levels of BCAR3 (shBCAR3-1), or ectopic Venus-BCAR3 in the

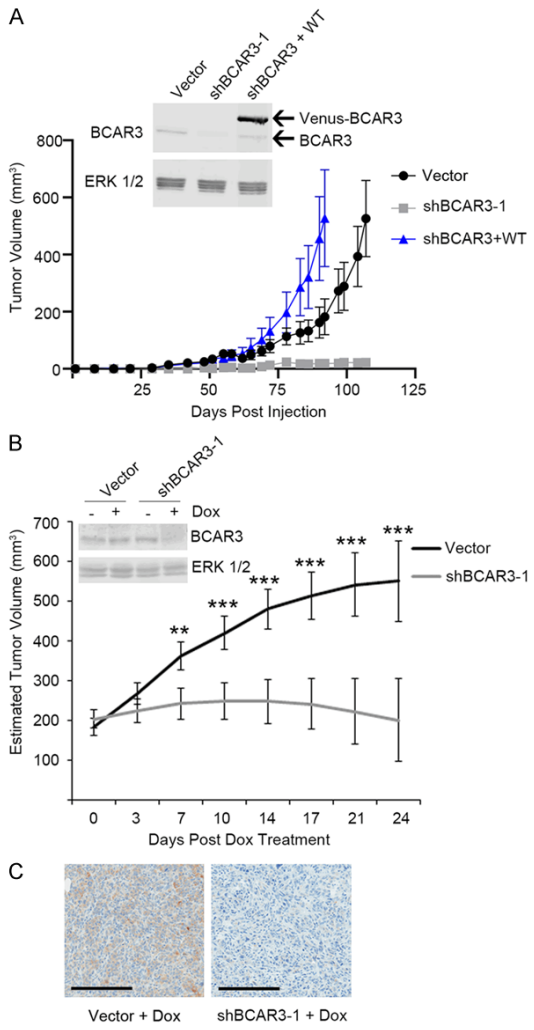

Figure 2. BCAR3 promotes tumor growth in orthotopic MDA-MB-231 mouse xenograft models. (A) 2×10^6 MDA-MB-231 cells were injected into both the left and right 4th inguinal mammary fat pad. Corresponding cells were lysed and immunoblotted for BCAR3 and ERK 1/2 to verify BCAR3 knockdown (shBCAR3-1) and re-expression of WT Venus-BCAR3 (shBCAR3 + WT) (inset). Tumors were measured by caliper 3 times a week. Data shown are the average +/- SEM of 15 control tumors, 13 shBCAR3-1 tumors and 13 shBCAR3 + WT tumors. A permutation test using 2000 permutations was used to determine *P*-values. (B) 2×10^6 Dox-inducible MDA-MB-231 control and BCAR3 knockdown cells were injected into the left and right 4th inguinal mammary fat pad. Corresponding cells were lysed and immunoblotted for BCAR3 and ERK 1/2 to verify regulated expression of BCAR3 under the shBCAR3 + Dox conditions (inset). Doxycyline was added to the animals' drinking water once the tumors reached 200 mm^3. The data represent an average of 10 (Vector) and 8 (shBCAR3-1) tumors. An F-test based on contrasts was used to compare groups and determine *P*-values. **indicates P<0.001, ***indicates P<0.0001. (C) Tumors were excised at the endpoint of the experiment, formalin fixed, embedded in paraffin, and stained for BCAR3.

background of the BCAR3 knockdown (shBCAR3 + WT) (**Figure 2A**, inset) were injected into the 4th inguinal fat pads of Foxn1$^{nu/nu}$ mice. While the control cells readily formed tumor masses, the shBCAR3-1 knockdown cells uniformly failed to produce measurable tumors (**Figure 2A**). This deficiency was reversed when ectopic Venus-BCAR3 was expressed in the shBCAR3-1 cells. In fact, tumor growth in cells with ectopic BCAR3 expression was significantly greater than in the presence of endogenous BCAR3, possibly due to the over-expression of Venus-BCAR3 relative to endogenous BCAR3 (see inset, **Figure 2A**; note that ectopic expression of Venus-BCAR3 may also stabilize endogenous BCAR3 as seen by the lower-migrating BCAR3 band).

We reasoned that the absence of tumor growth exhibited by shBCAR3-1 cells could be due to an inability of the cells to establish tumors and/or a decrease in tumor cell proliferation/survival in the mouse. To address these possibilities, tumor studies were repeated using a doxycycline (Dox)-inducible system to regulate expression of the shBCAR3 construct. Dox-inducible control and shBCAR3 MDA-MB-231 cells were inoculated as described above and Dox was introduced into the drinking water to knock down BCAR3 once tumors reached 200 mm^3. While the control tumors continued to grow in the presence of Dox, tumors generated from the conditional knockdown cells failed to progress once BCAR3 knockdown was initiated (**Figure 2B**). Immunohistochemistry performed on tumor samples isolated 24 days post-Dox treatment confirmed the knockdown of BCAR3 (**Figure 2C**). Together, these data strongly support a role for BCAR3 in promoting tumor growth *in vivo*.

BCAR3 promotes TNBC cell proliferation

To investigate a potential role for BCAR3 in TNBC cell proliferation, MDA-MB-231 cells containing either empty vector or one of two shBCAR3-encoding lentiviral constructs were plated at low density and growth was assessed every day for a period of 7 days using the CyQUANT assay. Western blot analysis confirmed knockdown of BCAR3 (**Figure 3A**, inset). Cell numbers were reduced under conditions of BCAR3 knockdown compared to control cells (**Figure 3A**). This effect appeared to be dependent on the expression level of BCAR3,

as the shBCAR3-1 cells that featured a more robust BCAR3 knockdown exhibited a greater deficiency in cell number than did the shBCAR3-2 cells that exhibited a more modest BCAR3 knockdown. To further assess the contribution of BCAR3 to cell proliferation, long-term growth assays were performed. Cells were plated at low density, allowed to grow for 10 days with no media changes, and stained with crystal violet. Colony growth as determined by the intensity of the crystal violet signal was significantly reduced in shBCAR3 cultures grown under these conditions and, similar to the previous experiment, inhibition of colony growth appeared slightly greater in the shBCAR3-1 cells than in the shBCAR3-2 cells (**Figure 3B**). This difference was unlikely to be due to cell death, as the number of viable cells at early times after plating (24 and 72 hours) was similar for Vector-control and shBCAR3-1 cells (**Figure 4A**).

To verify that the reduced colony size exhibited by BCAR3 knockdown cells was a consequence of BCAR3 depletion, constructs encoding shRNA-resistant ectopic Venus-BCAR3 (shBCAR3 + WT) or the empty vector (shBCAR3 + Ctl) were expressed in shBCAR3-1 cells (**Figure 3C**; again, note that ectopic expression of Venus-BCAR3 may stabilize endogenous BCAR3 as seen by the lower-migrating BCAR3 band). As before, colony growth was reduced in cells expressing lower amounts of BCAR3 (shBCAR3-1 and shBCAR3 + Ctl) (**Figure 3D**). However, this deficiency was largely alleviated when ectopic Venus-BCAR3 was expressed in the knockdown cells. A similar result was observed in a second TNBC cell line, Hs578T (**Figures 3E**, **3F**, and **4B**). Together, these data show that, under long-term growth conditions, BCAR3 promotes TNBC colony expansion.

BCAR3 is required for budding of mouse mammary epithelial organoids in response to growth factors

Mammary branching morphogenesis is a dynamic process involving cell proliferation, remodeling, and response to external cues [34, 35], all of which also contribute to TNBC tumor growth and progression. To further explore proliferation as a function of BCAR3 expression, we used a mouse mammary epithelial organoid system as a tool to measure mammary epithelial cell proliferation. Primary organoids were generated using epithelial cells isolated from mammary glands obtained from wildtype (WT) and BCAR3 knock-out (B3KO) mice (**Figure 5A**). Epithelial cells were suspended in Matrigel to establish primary mammary organoids and treated for 7 days with two growth factors that have historically been used to stimulate branching morphogenesis, fibroblast growth factor 2 (FGF2) and transforming growth factor α (TGFα) [27, 36] (**Figure 5B**). Organoid budding was then quantified as a measure of proliferation. Organoids generated from BCAR3 KO mice exhibited less budding when treated with FGF2 or TGFα compared to organoids generated from WT mice (**Figure 5C** and **5D**). BCAR3 KO organoids treated with FGF2, but not TGFα, were also smaller in size compared to those generated from WT mice (**Figure 5E**), suggesting that BCAR3 may modulate differential growth responses depending on the nature of external growth factors.

BCAR3-MET coupling regulates TNBC cell proliferation and migration

To gain a more complete understanding of the signaling pathways that might partner with BCAR3 to drive TNBC phenotypes, we performed gene set variation analysis (GSVA). Publicly available mRNA expression data from a panel of 32 TNBC cell lines in the Cancer Cell Line Encyclopedia (CCLE) were used to identify receptor tyrosine kinase gene sets whose enrichment correlated positively with BCAR3 transcript abundance. Fibroblast Growth Factor Receptor (FGFR) and Epidermal Growth Factor Receptor (EGFR) signaling pathways, which were shown to be impaired in the absence of BCAR3 for FGF2- and TGFα-induced organoid budding, respectively, were positively correlated with BCAR3 mRNA abundance (**Figure 6A**). In addition, gene sets associated with the MET receptor signaling showed a strong correlation with BCAR3 mRNA expression. MET was readily detected by Western blot analysis in both claudin-low and basal-like TNBC cells (see **Figure 1C**). This prompted us to investigate the potential role of MET in BCAR3-dependent cell proliferation. MDA-MB-231 and Hs578T cells were treated with 50 nM of the MET inhibitor, Foretinib; this concentration produces a significant reduction in MET autophosphorylation (pTyr1234/1235) following HGF stimulation

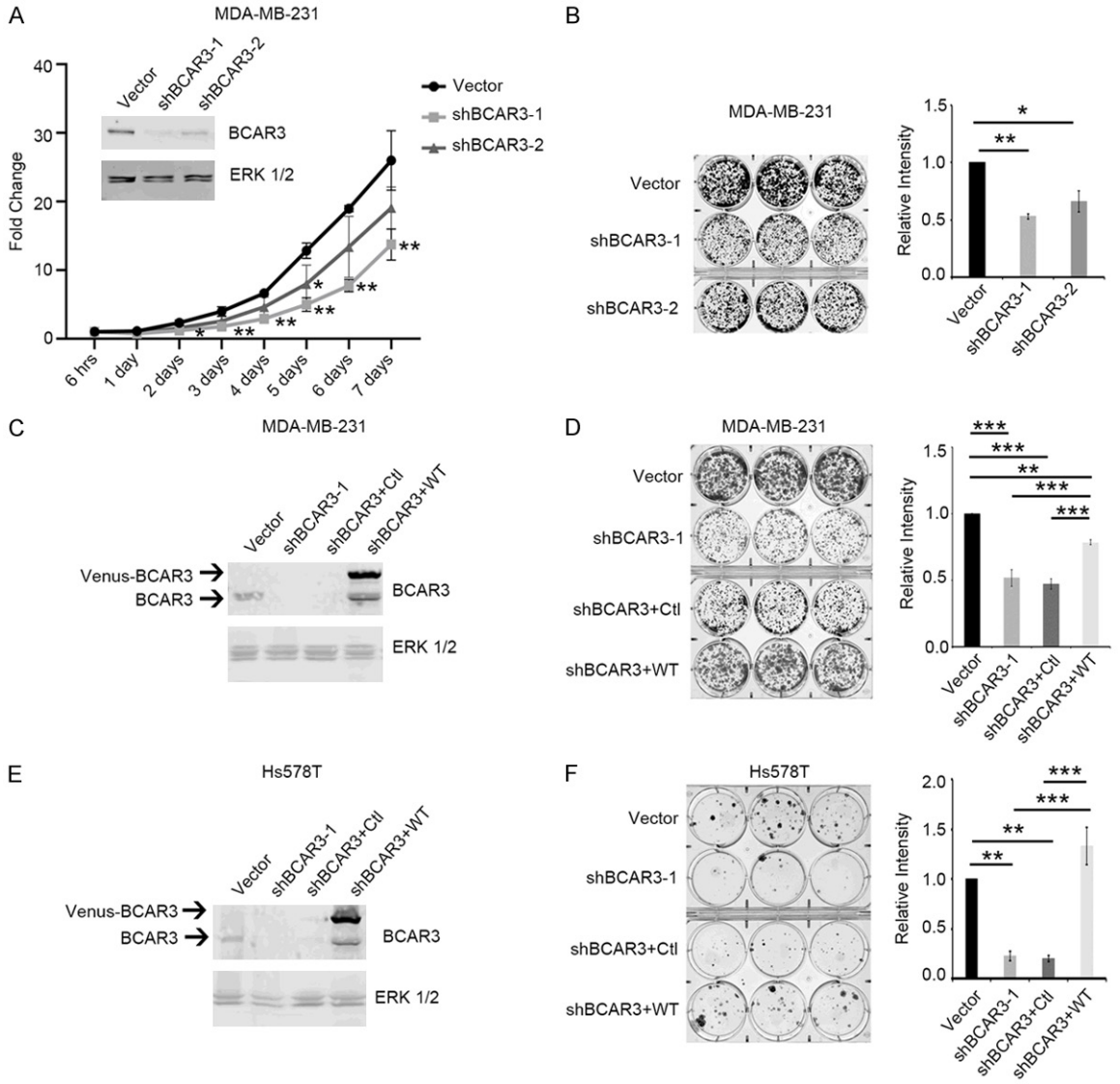

Figure 3. BCAR3 promotes TNBC cell proliferation. (A) CyQUANT NF cell proliferation assays were performed using control (Vector), shBCAR3-1 and shBCAR3-2 MDA-MB-231 cells. BCAR3 expression levels are shown in the inset. Each point on the graph represents the average fold change +/- SEM relative to a 6 hour baseline. Data were collected from 3 independent biological replicates. ANOVA analysis comparing the 3 cell lines for each day followed by a Tukey's post hoc test was used to determine *P*-values. (B) Long-term colony growth assays. 1000 cells/well were plated in triplicate in 6-well plates, allowed to grow for 10 days, and staining intensity was quantified. Data from the 3 technical replicates were averaged for each experiment and normalized to control cells. The average of 3 independent experiments +/- SEM was plotted on the graph. (C) Representative immunoblot showing endogenous BCAR3 and ectopic Venus-BCAR3 expression in the indicated MDA-MB-231 cell lines. (D) Cells were cultured in triplicate for 10 days and analyzed as described in (B). Data shown are the average +/- SEM of 5 independent experiments. (E) Representative immunoblot showing endogenous BCAR3 and ectopic Venus-BCAR3 expression in the indicated Hs578T cell lines. (F) Cells were cultured in triplicate for 15 days and analyzed as described for (B). Data shown are the average +/- SEM of 3 independent experiments. For all long-term colony growth assays, ANOVA analysis followed by Tukey's post hoc tests was used to determine *P*-values. *indicates P<0.05, **indicates P<0.01, ***indicates P<0.001.

(**Figure 7A**) and is 50-100-fold below the reported IC50 (dose at which there is a 50% reduction in cell survival) for MDA-MB-231 cells [37]. Importantly, neither Vector-control nor BCAR3-depleted cells demonstrated a loss in viability in the presence of 50 nM Foretinib during the early stages of this assay (**Figure 7B**). While MDA-MB-231 cells expressing the

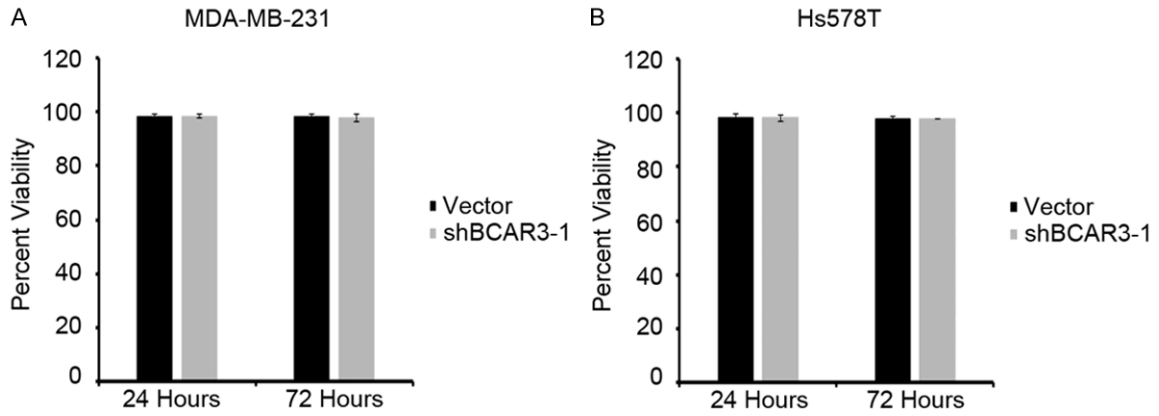

Figure 4. BCAR3 knockdown does not impact cell viability at 24 or 72 hours. MDA-MB-231 (A) or Hs578T (B) cells were cultured for a period of 24 or 72 hours. Viability was measured using Trypan Blue exclusion. Data shown are the average of 3-4 independent experiments. ANOVA followed by Sidak post hoc tests were used to determine differences.

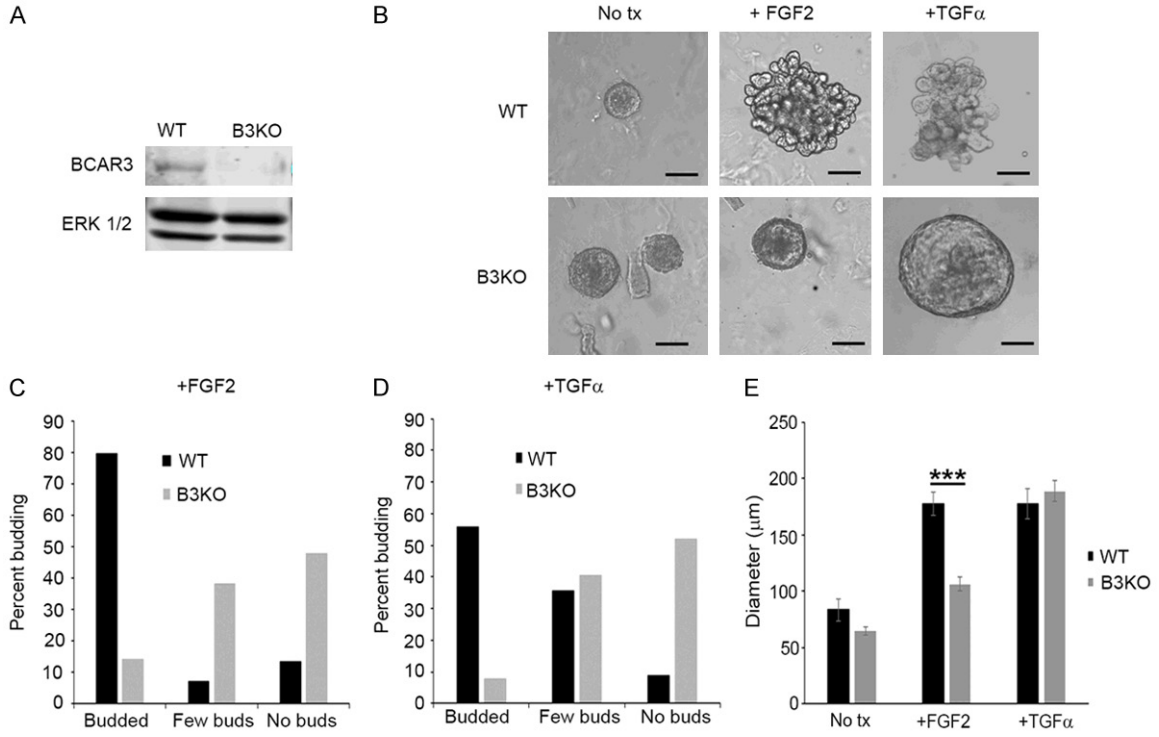

Figure 5. BCAR3 promotes budding of mammary organoids under conditions of FGF2 and TGFα treatment. (A) Representative immunoblot from organoids generated from 8-week old wildtype (WT) and BCAR3 knockout (B3KO) mice cultured *in vitro* for 7 days. (B) Representative images of organoids cultured in the absence (no tx) or presence of FGF2 (2.5 nm) or TGFα (9 nM) for 7 days. Scale bar represents 50 μm. (C and D) Quantification of organoids that exhibited robust budding (budded; >10), few buds (≤10 buds), or no buds. Data were generated from 1255 WT and 1015 B3KO organoids gathered from 7 independent experiments (FGF2), and 790 WT and 822 B3KO organoids gathered from 3 independent experiments (TGFα). Chi-squared tests were used to determine differences between groups ($P<0.001$). (E) The average diameter of organoids +/- SEM is shown for WT and B3KO organoids (37-46 organoids over multiple independent experiments) cultured under the indicated conditions. ANOVA followed by a Sidak post hoc test was used to determine differences. ***indicates $P<0.001$.

vector failed to exhibit a significant decrease in colony growth in the presence of Foretinib, colony growth of the analogous Hs578T cells was reduced under these conditions (**Figure**

6B; black bars). The greater sensitivity of Hs578T cells to Foretinib may be explained in part by the higher expression of MET receptor in these cells (see **Figure 1C**). However, although depletion of BCAR3 again resulted in a decrease in colony growth for both MDA-MB-231 and Hs578T cells (gray bars, no inhibitor), treatment of shBCAR3 cells with Foretinib did not cause any additional growth-inhibitory effect beyond what was observed in vehicle-treated cells. These data suggest that MET and BCAR3 may function in the same pathway to control cell growth, at least in the case of Hs578T cells where inhibition of MET alone caused a reduction in cell growth.

Considering that both the MET receptor and BCAR3 have been implicated in migration of cancer cells [13, 14], we next sought to explore whether these proteins functioned together to regulate cell migration. Vector-control and BCAR3-depleted MDA-MB-231 and Hs578T cells were plated in Boyden chambers and allowed to migrate toward HGF in the presence or absence of 50 nM Foretinib. Inhibition of MET in control cells reduced migration by approximately 40-50% (**Figure 6C**; black bars), similar to the reduced migration observed in BCAR3 knockdown cells in the absence of Foretinib (gray bar). However, as was the case for proliferation, Foretinib had no added effect beyond BCAR3 depletion alone, again supporting a model in which BCAR3 and MET function in the same regulatory pathway.

To further explore the functional relationship between BCAR3 and MET, we next examined MET receptor activation in cells plated for 2 to 10 days with no media changes. Phosphorylation of MET at Tyr1234/1235 was observed after 10 days in culture in MDA-MB-231 cells expressing endogenous BCAR3 (Vector) and in knockdown cells expressing high levels of ectopic Venus-BCAR3 (**Figure 8A**; lanes 9 and 12). While Hs578T cells containing the vector did not show a similar elevation of MET phosphorylation, BCAR3-depleted cells that re-expressed Venus-BCAR3 exhibited robust MET activation after 5 and 10 days in culture (**Figure 8B**, lanes 8 and 12). Note that the level of Venus-BCAR3 present in these cells is significantly elevated compared to endogenous BCAR3.

Based on these data, we hypothesized that BCAR3 may contribute to autocrine signaling through the MET receptor. To test this hypothesis, HGF mRNA levels were measured by quantitative real-time PCR (RT-PCR) in the full panel of MDA-MB-231 and Hs578T cells. As expected, BCAR3 transcripts were decreased in shBCAR3-1 cells and elevated in cells overexpressing Venus-BCAR3 (**Figure 8C**). MET transcript levels were not significantly impacted by BCAR3 depletion or overexpression in either cell line. HGF mRNA levels were below the level of detection in MDA-MB-231 cells. However, HGF mRNA was detectable in Hs578T cells, and shBCAR3-1 + WT cells expressing robust levels of Venus-BCAR3 harbored significantly elevated HGF mRNA. Thus, in the presence of elevated BCAR3, HGF mRNA is upregulated in Hs578T cells.

HGF promotes colony growth in Hs578T cells

In light of the evidence for BCAR3-MET functional coupling in both MDA-MB-231 and Hs578T cells and the possibility that the increase in HGF mRNA seen in Hs578T cells overexpressing BCAR3 may contribute to the enhanced proliferation seen under these conditions, we sought to determine whether exogenous HGF could rescue the defect in colony growth observed under conditions of BCAR3 depletion. We reasoned that, if MET activation was due to autocrine signaling in a BCAR3-dependent fashion, then exogenous HGF would at least partially rescue the phenotype caused by BCAR3 depletion. Vector-control and BCAR3-depleted MDA-MB-231 and Hs578T cells were cultured long-term in the presence or absence of 50 ng/ml HGF. Irrespective of BCAR3 status, the average colony growth of MDA-MB-231 cells was not impacted by exogenous HGF (**Figure 9A** and **9B**). HGF induced a slight increase in the average colony density of Hs578T Vector-control but not shBCAR3 cells.

Interestingly, the distinctive variability in colony size exhibited by Hs578T cells appeared to be augmented upon treatment with HGF (**Figure 9A**). This prompted us to enumerate the proportion of Hs578T colonies falling into small, average, and large sizes as defined by the top (large) and bottom (small) quartiles of colony size for untreated Vector-control cells. HGF treatment of the Vector-control cells resulted in a shift from average to smaller colonies (**Figure 9C**). One possible explanation for this increase

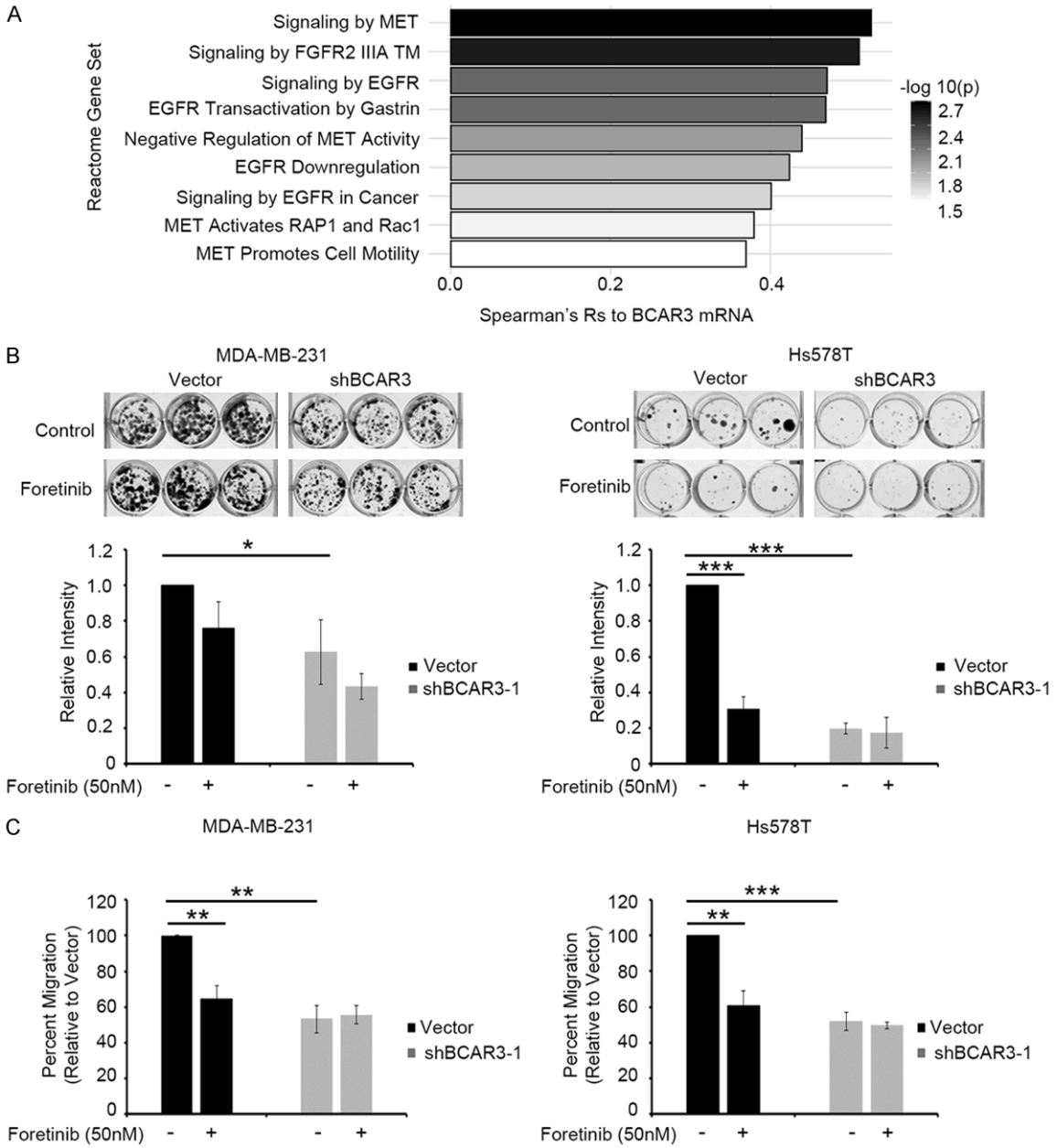

Figure 6. BCAR3 and MET function in the same proliferation and migration pathways. (A) Gene set variation analysis (GSVA) was used to calculate enrichment scores for the Reactome gene sets related to receptor tyrosine kinase signaling using mRNA transcript abundance data from 32 TNBC cell lines from the Cancer Cell Line Encyclopedia (CCLE). Spearman rank correlations and associated *P*-values ($-\log_{10}(p)$) were then calculated between the GSVA scores and BCAR3 transcript abundance from the same TNBC cell lines. (B) Long-term colony growth assays. 500 cells/well were plated in triplicate in 12-well plates and allowed to grow in the presence or absence of 50 nM Foretinib. MDA-MB-231 cells were treated with the inhibitor 24 hours post-plating, re-treated on days 3 and 6 after initial treatment, and stained at day 10. Hs578T cells were treated with inhibitor 24 hours post-plating, re-treated on day 3 after initial treatment, and stained at day 15. Staining intensity was quantified and data from 3 technical replicates were averaged for each experiment. Data were normalized relative to the DMSO-treated Vector-control sample and the average +/- SEM of 3 to 4 independent experiments was plotted on the graph. (C) Transwell migration assays. Percent migration of MDA-MB-231 and Hs578T cells toward 50 ng/ml HGF is shown. 25,000 cells were plated in the top well of Boyden chambers in the presence of DMSO or 50 nM Foretinib and incubated for 6 hours. Data shown are the average +/- SEM of 3 independent experiments. ANOVA followed by Sidak post hoc tests were used to determine differences. Asterisks indicate a significant difference from the Vector-control, no drug condition. *indicates P<0.05, **indicates P<0.01, ***indicates P<0.001.

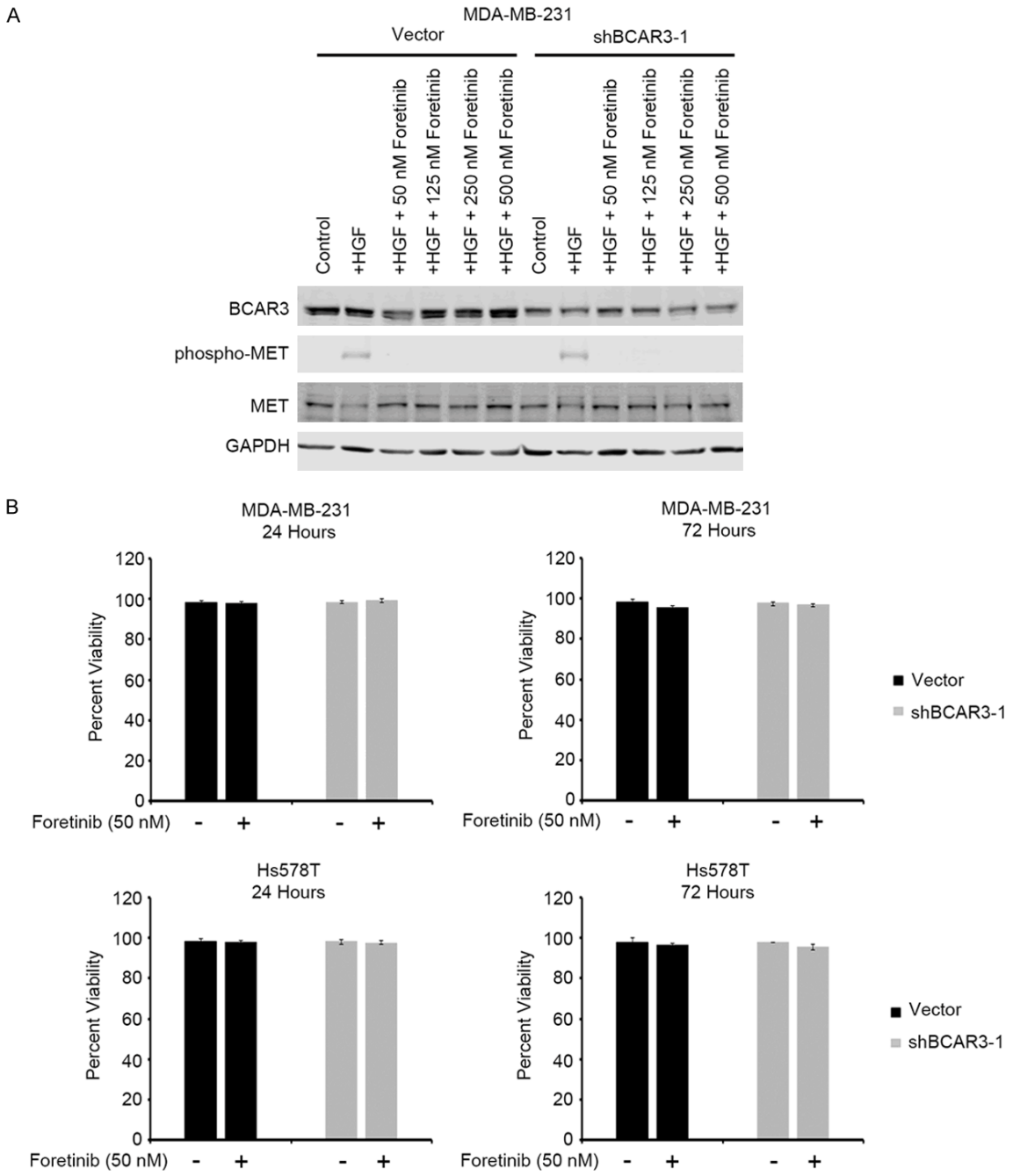

Figure 7. Foretinib inhibits MET receptor activation but does not impact viability at 50 nM. (A) Representative immunoblot from MDA-MB-231 cells treated as indicated. Phospho-MET antibodies recognize pTyr1234/1235. (B) Viability in the presence or absence of Foretinib was measured at 24 and 72 hours using Trypan Blue exclusion. Data shown are the average of 3-4 experiments +/- SEM. ANOVA followed by Sidak post hoc tests were used to determine differences.

in smaller colonies could be the "scatter" effect of HGF [38-40], leading to a more dispersed colony phenotype. In the shBCAR3 cells, HGF induced a bimodal change in colony size marked by an increase in both small and large colonies at the expense of the average cohort. This suggests that HGF may induce both scatter/migration of the shBCAR3 cells (leading to the colonies appearing smaller in size) as well as proliferation (leading to a larger colony size).

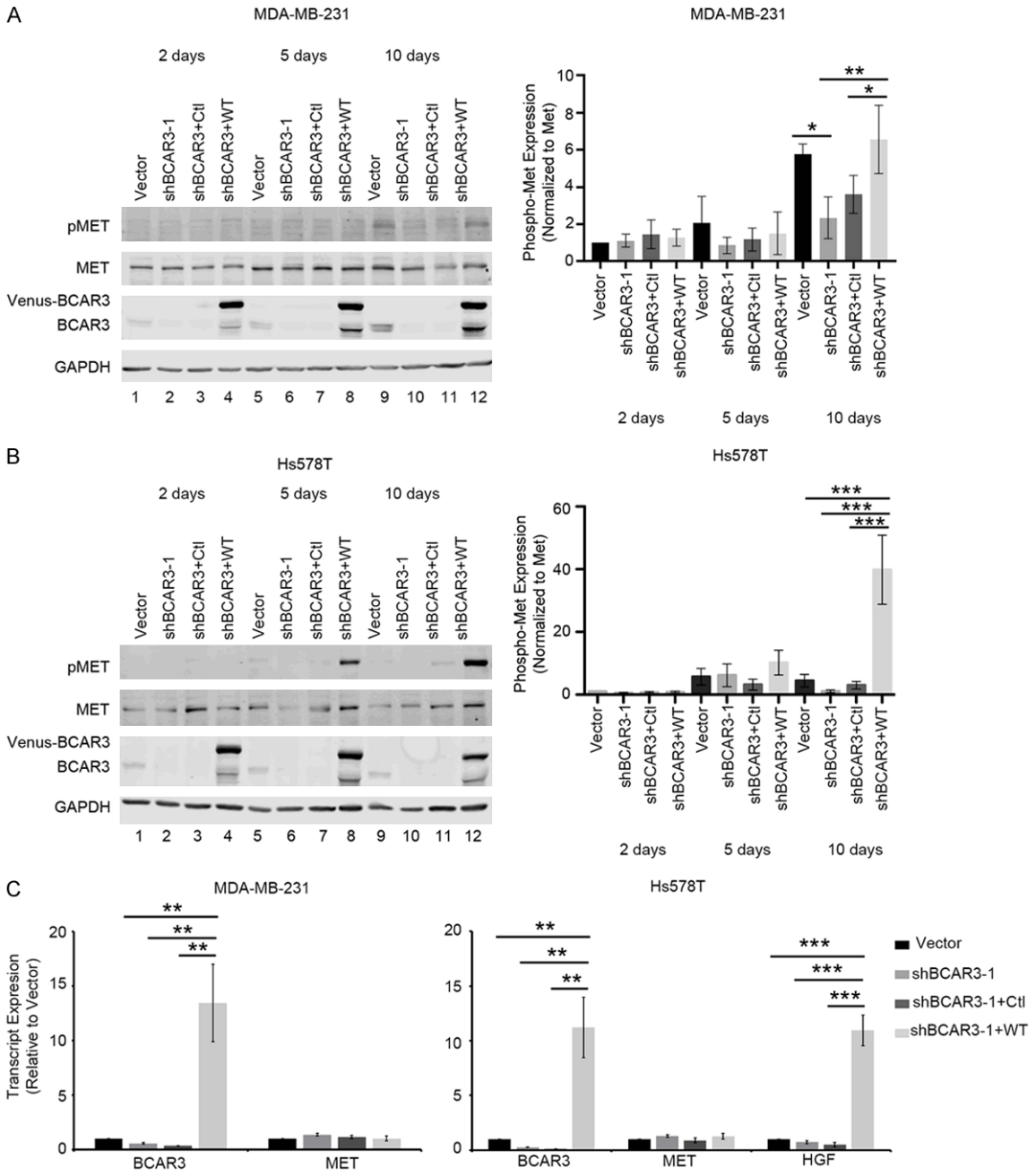

Figure 8. BCAR3 regulates MET receptor activation in cells cultured long-term. (A and B) Representative immunoblot analysis and quantification of MET activation in MDA-MB-231 (A) or Hs578T (B) cells with endogenous, depleted, or re-expressed BCAR3 expression. Cells were cultured for 2, 5, and 10 days with no media changes. Cells were lysed and protein expression/phosphorylation was evaluated with the indicated antibodies. Phospho-MET (Tyr1234/1235) was normalized to total MET and fold-change was quantified relative to Vector-control cells cultured for 2 days. (C) Quantitative real-time PCR analysis of BCAR3, MET and HGF transcript levels in the MDA-MB-231 and Hs578T cell panels cultured for 48 hours. RT-PCR was conducted with technical duplicates for 3 independent experiments. Data shown are the average +/- SEM of 3 biological replicates. ANOVA followed by Sidak post hoc tests were used to determine differences. *indicates P<0.05, **indicates P<0.01, ***indicates P<0.001.

While autocrine signaling through upregulation of HGF mRNA may contribute to BCAR3-dependent regulation of proliferation and migration in Hs578T cells, our data suggest that this is not the case for MDA-MB-231 cells. Instead, we hypothesized that MET receptor activation may be differentially regulated in Vector-control compared to shBCAR3 MDA-MB-231 cells. To

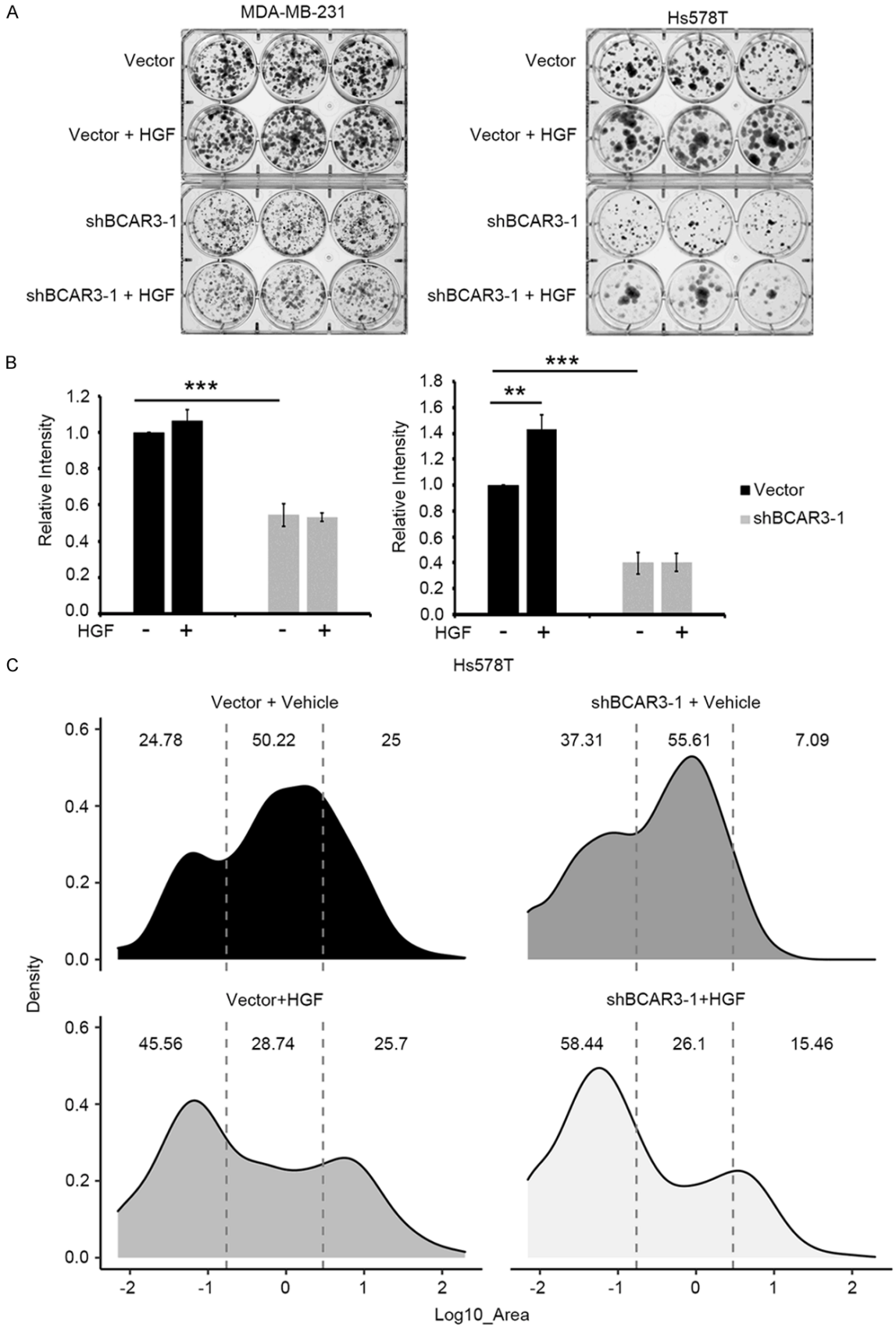
A
MDA-MB-231
Hs578T
Vector
Vector + HGF
shBCAR3-1
shBCAR3-1 + HGF
B
Relative Intensity
***
**
HGF
Vector
shBCAR3-1
Hs578T
C
Vector + Vehicle
shBCAR3-1 + Vehicle
Vector+HGF
shBCAR3-1+HGF
24.78
50.22
25
37.31
55.61
7.09
45.56
28.74
25.7
58.44
26.1
15.46
Density
Log10_Area

Figure 9. HGF treatment differentially impacts colony size distribution of Hs578T cells as a function of BCAR3. (A) Long-term colony growth assays under conditions of HGF stimulation. MDA-MB-231 and Hs578T cells were plated at a density of 1,000 cells/well in triplicate in a 6-well plate and treated with either vehicle (0.05% BSA) or 50 ng/mL HGF the day after plating. MDA-MB-231 cells were re-treated with HGF on days 3 and 6 after initial treatment and stained at day 10. Hs578T cells were re-treated with HGF on day 3 after initial treatment and stained at day 15. (B) Staining intensity was quantified and data from the 3 technical replicates were averaged for each experiment. Data were normalized relative to the vehicle-treated Vector-control sample and the average +/- SEM of 3 to 5 independent experiments was plotted on the graph. ANOVA followed by Sidak post hoc tests were used to determine *P*-values. (C) Quartile data obtained from the colony size distribution of untreated Vector-control cells were used to bin colonies into large (≥2.975 mm^2), average (<2.975 mm^2 ≥0.172 mm^2), or small (<0.172 mm^2) groupings. Data were generated from 904 Vector-control no treatment colonies, 856 Vector-control + HGF colonies, 1115 shBCAR3-1 no treatment colonies, and 705 shBCAR3-1 + HGF colonies obtained from 5 independent experiments. The chi-squared test was used to determine differences between groups (P<0.001). A test of 2-proportions was performed to compare small, average, and large colonies in cells of the same background treated with vehicle or HGF. The Holm method was used to correct for any errors that might have arisen from performing multiple tests across the comparisons analyzed. $P=3.26\times10^{-19}$ and 4.82×10^{-19} comparing vehicle to HGF-treated Vector-control cells for average and small colonies, respectively. $P=7.13\times10^{-18}$, 3.39×10^{-8}, 6.36×10^{-34} comparing vehicle to HGF treatment of shBCAR3 cells for small, large and average colonies, respectively.

test this hypothesis, MET phosphorylation at Tyr1234/1235 was measured following acute stimulation with HGF. Both the magnitude and duration of MET phosphorylation was attenuated under conditions of BCAR3 knockdown (**Figure 10A**), supporting a role for BCAR3 in regulating MET receptor activation in MDA-MB-231 cells.

Discussion

In this report, we used both *in vivo* and *in vitro* approaches to probe the function of BCAR3 in TNBC tumor growth, proliferation and migration. Our study is the first to show that BCAR3 regulates growth of TNBC xenografts in mouse models and that this correlates with its upregulation and association with poorer outcomes in patients with TNBC. In addition, we show that BCAR3-MET receptor coupling plays a key role in BCAR3-dependent proliferation and migration of TNBC cells, and that the mechanisms through which this functional interaction operates may differ in different genetic backgrounds of TNBC. Most importantly, these data open the possibility for new approaches to personalized therapy for individuals with TNBCs.

BCAR3 is a regulator of MET signaling

Like BCAR3, MET has been shown to drive cell proliferation, migration and invasion [13, 14]. It has also been shown to induce branching morphogenesis through its interaction with the adaptor molecule Gab1 [41]. Despite having similar functions in breast cancer, however, a connection between MET and BCAR3 has not been explored prior to this study. Using publicly available data, we showed that, among receptor tyrosine kinases, expression of the MET receptor signaling gene set correlated most strongly with BCAR3 mRNA expression in a panel of 32 TNBCs (**Figure 6A**). Our biological studies support a functional interaction between BCAR3 and MET that contributes to cell proliferation and migration (**Figure 6B** and **6C**). However, our data suggest that BCAR3-MET coupling may be mediated through distinct mechanisms in TNBCs depending on their genetic profiles. As suggested by **Figures 8C** and **9**, an autocrine loop generated through BCAR3-dependent expression of the MET receptor ligand HGF may help drive proliferation and migration of Hs578T cells (**Figure 10B**). Of note, studies have reported that exposure of luminal breast cancer cells to HGF induces increased growth with no morphological changes, while exposure of myoepithelial cells to HGF does not impact cell growth but rather induces morphological changes [42]. Considering that HGF elicits contrasting effects on luminal epithelial cells compared to myoepithelial cells, it will be interesting to compare the regulatory functions of BCAR3 on MET signaling between basal-like and claudin-low TNBC.

There is no evidence of autocrine signaling through BCAR3-MET receptor for MDA-MB-231 cells. While BCAR3 appears to be necessary in these cells for maximal MET receptor activation (**Figure 10A**), the inability of HGF to rescue the proliferation defect observed in BCAR3-depleted cells (**Figure 9B**) suggests that impairment of the BCAR3-MET axis under conditions of BCAR3 depletion may arise independently of ligand binding to the receptor (**Figure 10B**). Instead, BCAR3 could regulate the avail-

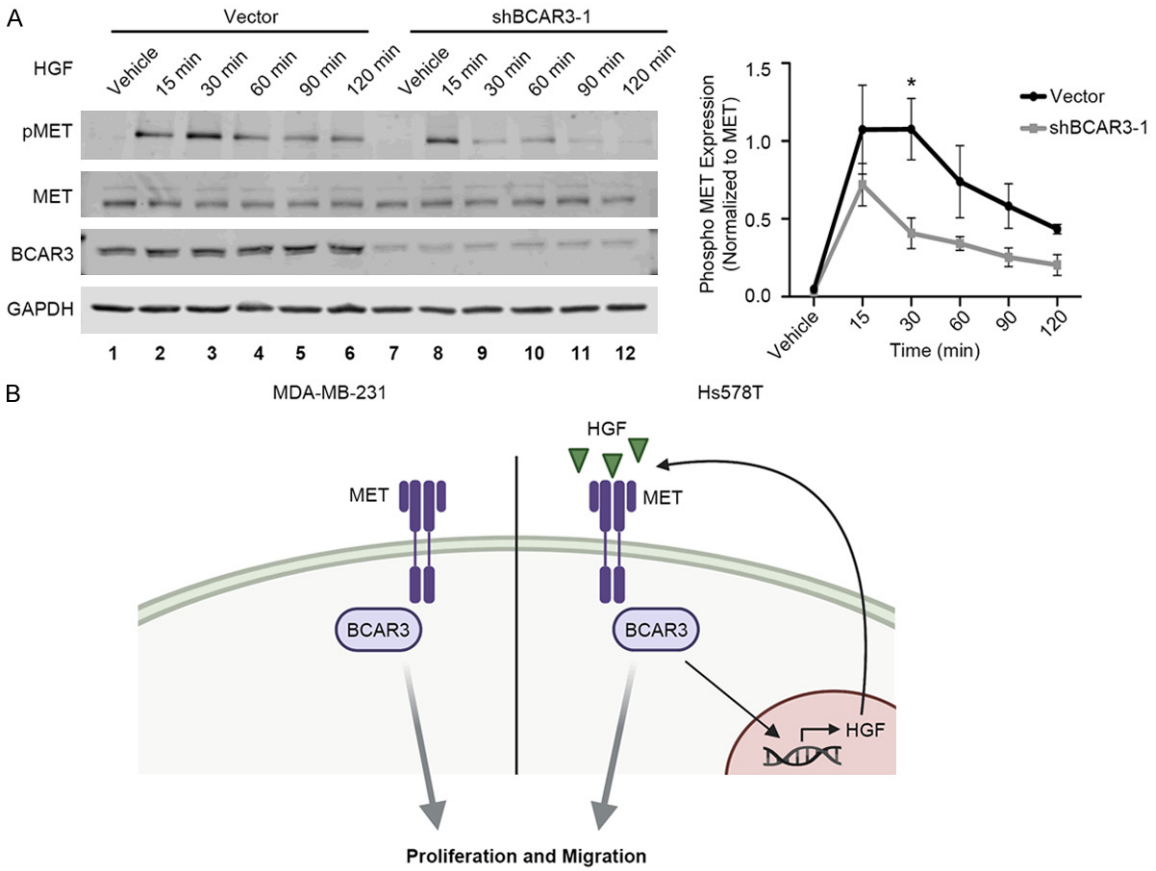

Figure 10. BCAR3-MET coupling in TNBC cells. (A) Representative immunoblot analysis of MDA-MB-231 cells with control or stable BCAR3 knockdown that were serum-starved and stimulated with 50 ng/mL HGF over a time-course ranging from 0-120 min. Cells were lysed and protein expression/phosphorylation was evaluated with the indicated antibodies. Data shown are the average ± SEM of 4 independent experiments. ANOVA followed by Sidak post hoc test was used to determine differences. Samples were derived from the same experiment and processed in parallel on multiple blots. *indicates $P<0.05$. (B) Model for functional BCAR3-MET coupling in MDA-MB-231 and Hs578T cells. Figure created with BioRender.com.

ability or activity of phosphatases, intracellular kinases, or adaptor molecules that control downstream signaling. While the mechanism through which this enhanced signaling is mediated through BCAR3 remains to be determined, the resultant increase in signal flux could account for the differences in cell migration and proliferation observed in MDA-MB-231 cells as a function of BCAR3.

Targeting BCAR3 signaling pathways for the treatment of TNBC

We have shown that BCAR3 expression is elevated in both ductal carcinoma in situ (DCIS) and invasive ductal carcinoma (IDC) compared to normal mammary tissue. Interestingly, the average BCAR3 expression was higher in DCIS than in IDC. Since BCAR3 is an important regulator of cell motility and invasion [1, 2, 12], its increased expression in a subset of DCIS lesions may reflect an early step in the transition to invasive disease. This possibility is further supported by the heterogeneity in BCAR3 expression that was observed in tumor tissue, suggestive of functional microdomains with high BCAR3 expression. Using publicly available patient data, we also found that high BCAR3 mRNA expression specifically in TNBC correlates with poorer outcomes. This is in contrast to several reports evaluating patients with hormone receptor-positive cancers that show that BCAR3 expression is a predictor of better outcomes [43, 44]. Our finding that BCAR3 protein expression was elevated in a subset of both TNBCs and ER+/PR+ tumors suggests that hormone status may help determine the impact of BCAR3 expression on the

tumor. Beyond hormone status alone, the fact that BCAR3 may function in different regulatory pathways even within individual TNBCs underscores the importance of also considering the receptor tyrosine kinases that coordinate with BCAR3 when developing personalized treatment strategies to control tumor progression for breast cancer patients. Our data provide the beginnings of a roadmap for this type of analysis by considering BCAR3-MET coupling as one axis to target therapeutically. Even more broadly, BCAR3 could serve as a potential biomarker for additional therapeutic avenues that exploit the distinct functional interactions through which BCAR3 contributes to tumor phenotypes. Further analysis of these interactions could help identify new molecular targets and drug combinations to enhance the clinical management of patients with TNBC.

Acknowledgements

The authors would like to thank the UVA Biorepository and Tissue Research Facility, the Research Histology Core, the Molecular Assessments and PreClinical Studies Core, the Biostatistics Shared Resources Core, and the Flow Cytometry Core; Mira Sridharan and Garvey Cummings for their input into experimental design and data interpretation; past and present lab members for their suggestions and comments; and Dr. Adam Lerner for providing us with BCAR3 knockout mice. This work was supported by grants from the Department of Defense Breast Cancer Research Program (W81XWH-15-1-0306) to AHB and the National Science Foundation (MCB 1716537) to MJL. JA was supported by T32 CA009109 and T32 GM007267, PJM was supported by T32 LM01-2416, and GV was supported by R25 CA2069-72. Additional support was provided by the UVA Cancer Center through P30 CA044579 (PI Loughran) and philanthropic funds. The authors state no conflicts of interest.

Disclosure of conflict of interest

None.

Address correspondence to: Amy H Bouton, Department of Microbiology, Immunology and Cancer Biology, University of Virginia School of Medicine and Cancer Center, P.O. Box 800734, Charlottesville, VA 22908, USA. Tel: 434-924-2513; E-mail: ahb8y@virginia.edu

References

[1] Cross AM, Wilson AL, Guerrero MS, Thomas KS, Bachir AI, Kubow KE, Horwitz AR and Bouton AH. Breast cancer antiestrogen resistance 3-p130Cas interactions promote adhesion disassembly and invasion in breast cancer cells. Oncogene 2016; 35: 5850-5859.

[2] Schrecengost RS, Riggins RB, Thomas KS, Guerrero MS and Bouton AH. Breast Cancer Antiestrogen Resistance-3 expression regulates breast cancer cell migration through promotion of p130Cas membrane localization and membrane ruffling. Cancer Res 2007; 67: 6174-6182.

[3] van Agthoven T, van Agthoven TL, Dekker A, van der Spek PJ, Vreede L and Dorssers LC. Identification of BCAR3 by a random search for genes involved in antiestrogen resistance of human breast cancer cells. EMBO J 1998; 17: 2799-2808.

[4] Garron ML, Arsenieva D, Zhong J, Bloom AB, Lerner A, O'Neill GM and Arold ST. Structural insights into the association between BCAR3 and Cas family members, an atypical complex implicated in anti-oestrogen resistance. J Mol Biol 2009; 386: 190-203.

[5] Mace PD, Wallez Y, Dobaczewska MK, Lee JJ, Robinson H, Pasquale EB and Riedl SJ. NSP-Cas protein structures reveal a promiscuous interaction module in cell signaling. Nat Struct Mol Biol 2011; 18: 1381-1387.

[6] Sun G, Cheng SY, Chen M, Lim CJ and Pallen CJ. Protein tyrosine phosphatase alpha phosphotyrosyl-789 binds BCAR3 to position Cas for activation at integrin-mediated focal adhesions. Mol Cell Biol 2012; 32: 3776-3789.

[7] Li C, Wang S, Xing Z, Lin A, Liang K, Song J, Hu Q, Yao J, Chen Z, Park PK, Hawke DH, Zhou J, Zhou Y, Zhang S, Liang H, Hung MC, Gallick GE, Han L, Lin C and Yang L. A ROR1-HER3-lncRNA signalling axis modulates the Hippo-YAP pathway to regulate bone metastasis. Nat Cell Biol 2017; 19: 106-119.

[8] Sakai R, Iwamatsu A, Hirano N, Ogawa S, Tanaka T, Nishida J, Yazaki Y and Hirai H. Characterization, partial purification, and peptide sequencing of p130, the main phosphoprotein associated with v-Crk oncoprotein. J Biol Chem 1994; 269: 32740-32746.

[9] Riggins RB, Quilliam LA and Bouton AH. Synergistic promotion of c-Src activation and cell migration by Cas and AND-34/BCAR3. J Biol Chem 2003; 278: 28264-28273.

[10] Schuh NR, Guerrero MS, Schrecengost RS and Bouton AH. BCAR3 regulates Src/p130Cas association, Src kinase activity, and breast cancer adhesion signaling. J Biol Chem 2010; 285: 2309-2317.

[11] Makkinje A, Vanden Borre P, Near RI, Patel PS and Lerner A. Breast Cancer Anti-estrogen Resistance 3 (BCAR3) protein augments binding of the c-Src SH3 domain to Crk-associated substrate (p130Cas). J Biol Chem 2012; 287: 27703-27714.

[12] Wilson AL, Schrecengost RS, Guerrero MS, Thomas KS and Bouton AH. Breast cancer antiestrogen resistance 3 (BCAR3) promotes cell motility by regulating actin cytoskeletal and adhesion remodeling in invasive breast cancer cells. PLoS One 2013; 8: e65678.

[13] Weidner KM, Sachs M and Birchmeier W. The MET receptor tyrosine kinase transduces motility, proliferation, and morphogenic signals of scatter factor/hepatocyte growth factor in epithelial cells. J Cell Biol 1993; 121: 145-154.

[14] Naldini L, Weidner KM, Vigna E, Gaudino G, Bardelli A, Ponzetto C, Narsimhan RP, Hartmann G, Zarnegar R, Michalopoulos GK, et al. Scatter factor and hepatocyte growth factor are indistinguishable ligands for the MET receptor. EMBO J 1991; 10: 2867-2878.

[15] Bottaro DP, Rubin JS, Faletto DL, Chan AM, Kmiecik TE, Vande Woude GF and Aaronson SA. Identification of the hepatocyte growth factor receptor as the c-met proto-oncogene product. Science 1991; 251: 802-804.

[16] Takayama H, LaRochelle WJ, Sharp R, Otsuka T, Kriebel P, Anver M, Aaronson SA and Merlino G. Diverse tumorigenesis associated with aberrant development in mice overexpressing hepatocyte growth factor/scatter factor. Proc Natl Acad Sci U S A 1997; 94: 701-706.

[17] Zagouri F, Bago-Horvath Z, Rossler F, Brandstetter A, Bartsch R, Papadimitriou CA, Dimitrakakis C, Tsigginou A, Papaspyrou I, Giannos A, Dimopoulos MA and Filipits M. High MET expression is an adverse prognostic factor in patients with triple-negative breast cancer. Br J Cancer 2013; 108: 1100-1105.

[18] Ponzo MG, Lesurf R, Petkiewicz S, O'Malley FP, Pinnaduwage D, Andrulis IL, Bull SB, Chughtai N, Zuo D, Souleimanova M, Germain D, Omeroglu A, Cardiff RD, Hallett M and Park M. MET induces mammary tumors with diverse histologies and is associated with poor outcome and human basal breast cancer. Proc Natl Acad Sci U S A 2009; 106: 12903-12908.

[19] Ghoussoub RA, Dillon DA, D'Aquila T, Rimm EB, Fearon ER and Rimm DL. Expression of c-met is a strong independent prognostic factor in breast carcinoma. Cancer 1998; 82: 1513-1520.

[20] Camp RL, Rimm EB and Rimm DL. Met expression is associated with poor outcome in patients with axillary lymph node negative breast carcinoma. Cancer 1999; 86: 2259-2265.

[21] Raghav KP, Wang W, Liu S, Chavez-MacGregor M, Meng X, Hortobagyi GN, Mills GB, Meric-Bernstam F, Blumenschein GR Jr and Gonzalez-Angulo AM. cMET and phospho-cMET protein levels in breast cancers and survival outcomes. Clin Cancer Res 2012; 18: 2269-2277.

[22] Jin L, Fuchs A, Schnitt SJ, Yao Y, Joseph A, Lamszus K, Park M, Goldberg ID and Rosen EM. Expression of scatter factor and c-met receptor in benign and malignant breast tissue. Cancer 1997; 79: 749-760.

[23] Yamashita J, Ogawa M, Yamashita S, Nomura K, Kuramoto M, Saishoji T and Shin S. Immunoreactive hepatocyte growth factor is a strong and independent predictor of recurrence and survival in human breast cancer. Cancer Res 1994; 54: 1630-1633.

[24] Dill EA, Gru AA, Atkins KA, Friedman LA, Moore ME, Bullock TN, Cross JV, Dillon PM and Mills AM. PD-L1 expression and intratumoral heterogeneity across breast cancer subtypes and stages: an assessment of 245 primary and 40 metastatic tumors. Am J Surg Pathol 2017; 41: 334-342.

[25] Gyorffy B, Lanczky A, Eklund AC, Denkert C, Budczies J, Li Q and Szallasi Z. An online survival analysis tool to rapidly assess the effect of 22,277 genes on breast cancer prognosis using microarray data of 1,809 patients. Breast Cancer Res Treat 2010; 123: 725-731.

[26] Near RI, Smith RS, Toselli PA, Freddo TF, Bloom AB, Vanden Borre P, Seldin DC and Lerner A. Loss of AND-34/BCAR3 expression in mice results in rupture of the adult lens. Mol Vis 2009; 15: 685-699.

[27] Nguyen-Ngoc KV, Shamir ER, Huebner RJ, Beck JN, Cheung KJ and Ewald AJ. 3D culture assays of murine mammary branching morphogenesis and epithelial invasion. Methods Mol Biol 2015; 1189: 135-162.

[28] Hanzelmann S, Castelo R and Guinney J. GSVA: gene set variation analysis for microarray and RNA-seq data. BMC Bioinformatics 2013; 14: 7.

[29] Jassal B, Matthews L, Viteri G, Gong C, Lorente P, Fabregat A, Sidiropoulos K, Cook J, Gillespie M, Haw R, Loney F, May B, Milacic M, Rothfels K, Sevilla C, Shamovsky V, Shorser S, Varusai T, Weiser J, Wu G, Stein L, Hermjakob H and D'Eustachio P. The reactome pathway knowledgebase. Nucleic Acids Res 2020; 48: D498-D503.

[30] Albert PS and Shih JH. Modeling tumor growth with random onset. Biometrics 2003; 59: 897-906.

[31] Saunus JM, Smart CE, Kutasovic JR, Johnston RL, Kalita-de Croft P, Miranda M, Rozali EN, Vargas AC, Reid LE, Lorsy E, Cocciardi S, Se-

idens T, McCart Reed AE, Dalley AJ, Wockner LF, Johnson J, Sarkar D, Askarian-Amiri ME, Simpson PT, Khanna KK, Chenevix-Trench G, Al-Ejeh F and Lakhani SR. Multidimensional phenotyping of breast cancer cell lines to guide preclinical research. Breast Cancer Res Treat 2018; 167: 289-301.

[32] Olsson E, Winter C, George A, Chen Y, Torngren T, Bendahl PO, Borg A, Gruvberger-Saal SK and Saal LH. Mutation screening of 1,237 cancer genes across six model cell lines of basal-like breast cancer. PLoS One 2015; 10: e0144528.

[33] Neve RM, Chin K, Fridlyand J, Yeh J, Baehner FL, Fevr T, Clark L, Bayani N, Coppe JP, Tong F, Speed T, Spellman PT, DeVries S, Lapuk A, Wang NJ, Kuo WL, Stilwell JL, Pinkel D, Albertson DG, Waldman FM, McCormick F, Dickson RB, Johnson MD, Lippman M, Ethier S, Gazdar A and Gray JW. A collection of breast cancer cell lines for the study of functionally distinct cancer subtypes. Cancer Cell 2006; 10: 515-527.

[34] Simian M, Hirai Y, Navre M, Werb Z, Lochter A and Bissell MJ. The interplay of matrix metalloproteinases, morphogens and growth factors is necessary for branching of mammary epithelial cells. Development 2001; 128: 3117-3131.

[35] Kessenbrock K, Smith P, Steenbeek SC, Pervolarakis N, Kumar R, Minami Y, Goga A, Hinck L and Werb Z. Diverse regulation of mammary epithelial growth and branching morphogenesis through noncanonical Wnt signaling. Proc Natl Acad Sci U S A 2017; 114: 3121-3126.

[36] Ewald AJ, Brenot A, Duong M, Chan BS and Werb Z. Collective epithelial migration and cell rearrangements drive mammary branching morphogenesis. Dev Cell 2008; 14: 570-581.

[37] Simiczyjew A, Dratkiewicz E, Van Troys M, Ampe C, Styczen I and Nowak D. Combination of EGFR inhibitor Lapatinib and MET inhibitor Foretinib inhibits migration of triple negative breast cancer cell lines. Cancers (Basel) 2018; 10: 335.

[38] Grotegut S, von Schweinitz D, Christofori G and Lehembre F. Hepatocyte growth factor induces cell scattering through MAPK/Egr-1-mediated upregulation of snail. EMBO J 2006; 25: 3534-3545.

[39] Zhu H, Naujokas MA and Park M. Receptor chimeras indicate that the MET tyrosine kinase mediates the motility and morphogenic responses of hepatocyte growth/scatter factor. Cell Growth Differ 1994; 5: 359-366.

[40] Weidner KM, Behrens J, Vandekerckhove J and Birchmeier W. Scatter factor: molecular characteristics and effect on the invasiveness of epithelial cells. J Cell Biol 1990; 111: 2097-2108.

[41] Weidner KM, Di Cesare S, Sachs M, Brinkmann V, Behrens J and Birchmeier W. Interaction between Gab1 and the c-MET receptor tyrosine kinase is responsible for epithelial morphogenesis. Nature 1996; 384: 173-176.

[42] Niranjan B, Buluwela L, Yant J, Perusinghe N, Atherton A, Phippard D, Dale T, Gusterson B and Kamalati T. HGF/SF: a potent cytokine for mammary growth, morphogenesis and development. Development 1995; 121: 2897-2908.

[43] van Agthoven T, Sieuwerts AM, Meijer-van Gelder ME, Look MP, Smid M, Veldscholte J, Sleijfer S, Foekens JA and Dorssers LC. Relevance of breast cancer antiestrogen resistance genes in human breast cancer progression and tamoxifen resistance. J Clin Oncol 2009; 27: 542-549.

[44] Guo J, Canaff L, Rajadurai CV, Fils-Aime N, Tian J, Dai M, Korah J, Villatoro M, Park M, Ali S and Lebrun JJ. Breast cancer anti-estrogen resistance 3 inhibits transforming growth factor b/SMAD signaling and associates with favorable breast cancer disease outcomes. Breast Cancer Res 2014; 16: 476.